Correlation between structural and magnetic properties of $La_{7/8}Sr_{1/8}Mn_{1-\gamma}O_{3+\delta}$ with controlled nonstoichiometry

2007 J. Phys.: Condens. Matter 19 016003

(http://iopscience.iop.org/0953-8984/19/1/016003)

INSTITUTE OF PHYSICS PUBLISHING JOURNAL OF PHYSICS: CONDENSED MATTER

J. Phys.: Condens. Matter **19** (2007) 016003 (12pp) doi:10.1088/0953-8984/19/1/016003

Correlation between structural and magnetic properties of $La_{7/8}Sr_{1/8}Mn_{1-\gamma}O_{3+\delta}$ with controlled nonstoichiometry

H F Li[1], Y Su[1], J Persson[1], P Meuffels[1], J M Walter[2], R Skowronek[2] and Th Brückel[1]

[1] Institut für Festkörperforschung, Forschungszentrum Jülich GmbH, D-52425 Jülich, Germany
[2] Neutron Diffraction Group of the Mineralogic-Petrological Institute of Bonn University, Research Center Jülich GmbH, MIN/ZFR, D-52425 Jülich, Germany

Received 18 August 2006, in final form 10 November 2006
Published 7 December 2006
Online at stacks.iop.org/JPhysCM/19/016003

Abstract

The structural and magnetic properties of air sintered and Ar and O_2 annealed $La_{0.875}Sr_{0.125}Mn_{1-\gamma}O_{3+\delta}$ polycrystalline samples have been studied systematically. From the simultaneous refinement of room-temperature x-ray and neutron powder diffraction data, we have found that the crystal structure is orthorhombic ($Pbnm$, Z = 4; O) for the Ar annealed sample and rhombohedral ($R\bar{3}c$, Z = 2; R) for the air sintered and O_2 annealed samples. At the O–R transition, the average Mn–O–Mn bond angle increases from 161.08(4)° (Ar) to 163.38(1)° (O_2) and 163.64(1)° (air). Ar and O_2 annealings cause a decrease of the Curie temperature T_c from 240(1) K (air) via 237(1) K (O_2) to 192(1) K (Ar). The T_c is reduced by ∼20% for the sample with O structure (Ar) as compared with that of the samples with R structure (air and O_2). The decrease of T_c is explained by the decrease of total strength of magnetic interactions, due to the decreased ⟨Mn–O–Mn⟩ bond angle and increased ⟨Mn–O⟩ bond length, and by the decrease of number of nearest magnetic neighbours. The possible reasons for the decrease of the Mn site occupancy after Ar and O_2 annealings and the sources of apparent excess oxygen are discussed. Thus we have shown that the actual distributions of cation vacancies in the A (La and Sr) and B (Mn) sublattices induced by the changes of Mn and oxygen contents through Ar and O_2 annealings play an important role in the structural and magnetic properties. Comparing the Ar annealed with the air sintered sample, a decrease as small as ∼2.2% of the relative oxygen content leads to a remarkably large (∼20%) effect on T_c.

1. Introduction

$La_{1-x}Sr_xMnO_3$ is one of the most interesting systems in doped perovskite-type oxides due to its rich structural, magnetic and electronic properties that are governed by the interplay of lattice,

spin, charge and orbital degrees of freedom. The colossal magnetoresistance (CMR) effect is its extraordinary property. Polycrystals, single crystals and thin films of $La_{1-x}Sr_xMnO_3$ have been extensively studied [1–10, 13–19], not only because of the exciting physics but also because of the potential application, e.g. as cathode materials for solid fuel cells and a new class of memory devices.

Recently Hemberger *et al* [1] have reported the phase diagram of $La_{1-x}Sr_xMnO_3$ single crystals. For nominal doping $x = 0.125$, the single crystal has an O structure [2, 3], but for polycrystalline samples, depending on the preparation methods, different authors [4, 5] have reported O and R structures. Dutta *et al* [6] have reported the synthesis of nanoparticle $La_{0.875}Sr_{0.125}MnO_3$ samples that have the R structure using the sol–gel method. The structural transitions as a function of temperature for a $La_{0.875}Sr_{0.125}MnO_3$ single crystal have been reported. At ∼450 K, a transition from a high-temperature R to an O structure occurs. At ∼270 K, the O structure distorts to the Jahn–Teller distorted orthorhombic (O′) phase. Finally O′ transforms into another orthorhombic (O″) structure at ∼140 K [7]. Below $T_c \approx 180$ K, a ferromagnetic metallic phase appears and then transforms into a ferromagnetic insulator (FMI) at the temperature of the O′–O″ transition that is thought to be connected with the charge and orbital order [2, 3, 7, 8], and the magnetization shows a sudden increase at this temperature. The nature of FMI state is still debated [2, 3, 8–10]. Besides the peculiar physical properties, the defect chemistry such as cation nonstoichiometry and excess oxygen is also a crucial issue for the understanding of manganites because it determines the temperature of the O–R transition and the value of T_c, etc. Sublimation of metal ions or their compounds during the high-temperature reactions is unavoidable and excess oxygen in this composition usually exists with normal preparation methods. Taking into account these problems, the relative percentage of Mn^{3+} and Mn^{4+} ions, in principle, is governed by the substitutional doping, excess oxygen and cation deficiency. Thus the chemical formula of samples with the nominal composition $La_{1-x}Sr_xMnO_3$ should be expressed as $La_{1-x-\alpha}Sr_{x-\beta}Mn_{1-\gamma}O_{3+\delta}$. Based on the charge neutrality condition, the hole concentration is $(x + 2\delta + 3\alpha + 2\beta + 3\gamma)$, if we assume the usual ionic picture with integer valencies.

To determine the oxygen content in manganites, one of the popular methods is the high sensitivity thermogravimetric analysis (TGA), where one must obtain a fixed point for the normalization of oxygen content. Thus the measured oxygen content is relative and not absolute. The second method is iodometric titration, which determines the average chemical compositions; its accuracy is strongly affected by the homogenization and purity of the measured sample. Another useful method is high-resolution neutron powder diffraction because of the differences between the neutron scattering lengths of different elements.

In this paper, annealings with Ar and O_2 gases for $La_{7/8}Sr_{1/8}MnO_3$ were performed at 1 atm to change the oxygen content while keeping the same cation composition. We report the simultaneous Rietveld refinement combining both the room-temperature neutron and x-ray powder diffraction data and the magnetic properties of air sintered, and Ar and O_2 annealed samples. A complete neutron diffraction study of the structural transition, magnetic order and coherent Jahn–Teller distortion in the Ar annealed and air sintered samples from 10 to 900 K will be published elsewhere.

2. Experimental details

Polycrystalline samples of $La_{0.875}Sr_{0.125}Mn_{1-\gamma}O_{3+\delta}$ were synthesized from stoichiometric mixtures of La_2O_3 (99.99%), MnO_2 (99.9%) and $SrCO_3$ (99.999%). After mixing and milling, the raw materials were calcined twice at 1373 K for 12 h in air in order to carry out decarbonization and pre-reaction. The resultant black powder was isostatically pressed into

a cylindrical rod with a pressure of 54 MPa. After sintering two times at 1573 and 1623 K for 18 h at each temperature in air, two thirds of the product was then pressed into two cylindrical rods that were annealed at 1273 K for 24 h in flowing gases of high purity argon and oxygen at 1 atm, respectively. Mixing and milling using balls after each firing and isostatic pressing led to dense and homogenous samples and ensured a complete reaction.

Powder samples for structural studies were obtained by carefully crushing the twice sintered, Ar and O_2 annealed rods. Neutron powder diffraction (NPD) data were collected in the angular range $2\theta = 0°$–$90°$ with a step size $0.1°$ and a constant wavelength 1.0959 Å on the powder diffractometer SV7-a at the FRJ-2 reactor in Jülich, Germany [11], complemented by x-ray powder diffraction (XPD) from the same samples. Both experiments were carried out at room temperature. The dc magnetization measurements between 5 and 400 K were carried out on a Quantum Design MPMS-7 superconducting quantum interference device (SQUID) magnetometer. The zero-field cooling (ZFC) and field cooling (FC) curves were obtained at applied fields of 20 and 60 Oe. The estimation of cations in the samples was carried out by inductively coupled plasma with optical emission spectroscopy (ICP-OES) analysis.

3. Structural studies

Structural parameters were determined from the joint refinement of XPD and NPD data using the Fullprof program [12] for three $La_{0.875}Sr_{0.125}Mn_{1-\gamma}O_{3+\delta}$ samples. The ICP-OES results show that there is almost no deviation of the La and Sr contents from the stoichiometry (table 1). Refinements for the relative Sr site occupancy while keeping the sum of the La and Sr site occupancies fixed at 1 give a composition of 0.125 for Sr within the estimated standard deviation (e.s.d.) for all samples. Therefore the La and Sr site occupancies were fixed to the stoichiometric values during the refinements.

The crystal structure is orthorhombic ($Pbnm$, Z = 4; O) for the Ar annealed sample and hexagonal ($R\bar{3}c$, Z = 6; H) for the air sintered and O_2 annealed samples. We transformed the parameters from H into R setting while analysing the data. The neutron and x-ray powder diffraction patterns of three samples are shown in figures 1(A) and (B), respectively, together with the calculated patterns and the differences between them. Insets show magnified NPD and XPD patterns of the Ar annealed and air sintered samples in selected 2θ regions. One may observe three Bragg reflections, i.e. (400), (224) and (040) in the NPD pattern (figure 1(a)), and one (111) in the XPD pattern (figure 1(a′)) for the Ar annealed sample. For the air sintered sample, the three reflections degenerate into two reflections (220) and (208) (figure 1(b)), and the (111) reflection disappears (figure 1(b′)). This shows that the Ar annealed sample has an O structure, while the air sintered and O_2 annealed samples belong to the R structure.

Refined structural parameters of three $La_{0.875}Sr_{0.125}Mn_{1-\gamma}O_{3+\delta}$ samples are summarized in table 1, together with the measured (ICP-OES) cationic contents. The low values of reliability factors represent the good Rietveld refinements. The refined cationic site occupancies are in agreement with the cationic contents obtained from the ICP-OES analysis within the experimental errors. Table 1 shows that the oxygen site occupancy decreases by ∼2.2% and increases by ∼1.7% for the Ar and O_2 annealed samples, respectively, compared with that of the air sintered sample. At the same time the Mn site occupancy seems to decrease by ∼2.7% after the Ar annealing. This suggests that the flowing gas of Ar and O_2 decreases and increases the oxygen site occupancy during annealings, respectively. Simultaneously, Ar can carry some sublimational metal ions or their compounds out, especially for Mn ions. For three samples, the ⟨Mn–O⟩ bond length decreases from 1.982(2) Å (Ar) to 1.968(1) Å (O_2) and 1.965(1) Å (air), while the ⟨La(Sr)–O⟩ distance also decreases from 2.776(2) Å (Ar) to 2.761(1) Å (O_2) and 2.758(1) Å (air), thus resulting in the decrease of unit-cell volume V

Table 1. Refined structural parameters of the Ar annealed, air sintered and oxygen annealed $La_{0.875}Sr_{0.125}Mn_{1-\gamma}O_{3+\delta}$ samples at room temperature as obtained from refinements of combined XPD and NPD data. μ represents the refined site occupancy or the measured (ICP-OES) cationic content. Numbers in parentheses are the estimated standard deviation (e.s.d.) of the last significant digit.

Synthesis	Ar		Air		O_2	
Crystal system	O		R		R	
Space group	$Pbnm$		$R\bar{3}c$		$R\bar{3}c$	
La/Sr	4c		2a		2a	
x	0.0022(3)		0.25		0.25	
y	0.0212(4)		0.25		0.25	
B(La/Sr) (Å^2)	0.85(4)		0.81(4)		0.58(4)	
μ_{refining} (La)	0.875		0.875		0.875	
$\mu_{\text{ICP-OES}}$ (La)	0.88(1)		0.88(1)		0.88(1)	
μ_{refining} (Sr)	0.125		0.125		0.125	
$\mu_{\text{ICP-OES}}$ (Sr)	0.12(1)		0.12(1)		0.12(1)	
Mn	4b		2b		2b	
B(Mn) (Å^2)	0.36(7)		0.31(7)		0.15(7)	
μ_{refining} (Mn)	0.960(8)		0.986(8)		0.985(8)	
$\mu_{\text{ICP-OES}}$ (Mn)	0.97(1)		0.98(1)		0.97(1)	
O1	4c		6e		6e	
x	0.0622(9)		0.6994(1)		0.6986(1)	
y	0.4930(4)		0.8006(1)		0.8014(1)	
B(O1) (Å^2)	1.23(4)		1.20(3)		1.11(3)	
μ_{refining} (O1)	1.044(3)		3.090(2)		3.144(8)	
O2	8d		—		—	
x	0.7305(9)		—		—	
y	0.2763(8)		—		—	
z	0.0332(4)		—		—	
B(O2) (Å^2)	1.35(9)		—		—	
μ_{refining} (O2)	1.980(3)		—		—	
a (Å)	5.5457(1)		5.4771(1)		5.4805(1)	
b (Å)	5.5249(1)		—		—	
c (Å)	7.8009(1)		—		—	
α_{rhomb} (deg)	—		60.613(1)		60.632(1)	
V_{cell}/Mn (Å^3)	59.75(2)		58.90(1)		59.03(1)	
⟨La(Sr)–O⟩ (Å)	2.776(2)		2.758(1)		2.761(1)	
Mn–O(1) (Å)	1.9809(9)					
Mn–O(2) (Å)	2.008(5)					
	1.957(5)					
⟨Mn–O⟩ (Å)	1.982(2)		1.965(1)		1.968(1)	
Mn–O(1)–Mn (deg)	159.82(4)					
Mn–O(2)–Mn (deg)	161.71(9)					
⟨Mn–O–Mn⟩ (deg)	161.08(4)		163.64(1)		163.38(1)	
Reliability factors	NPD	XRD	NPD	XRD	NPD	XRD
R_{p} (%)	3.08	2.68	2.77	2.67	2.66	2.66
R_{wp} (%)	4.37	3.44	3.90	3.37	3.77	3.39
χ^2	3.32		2.84		2.65	

per Mn ion from 59.75(2) Å^3 (Ar) to 59.03(1) Å^3 (O_2) and 58.90(1) Å^3 (air) (table 1). At the O–R transition, the ⟨Mn–O⟩, ⟨La(Sr)–O⟩ and V per Mn ion decrease. The mismatch

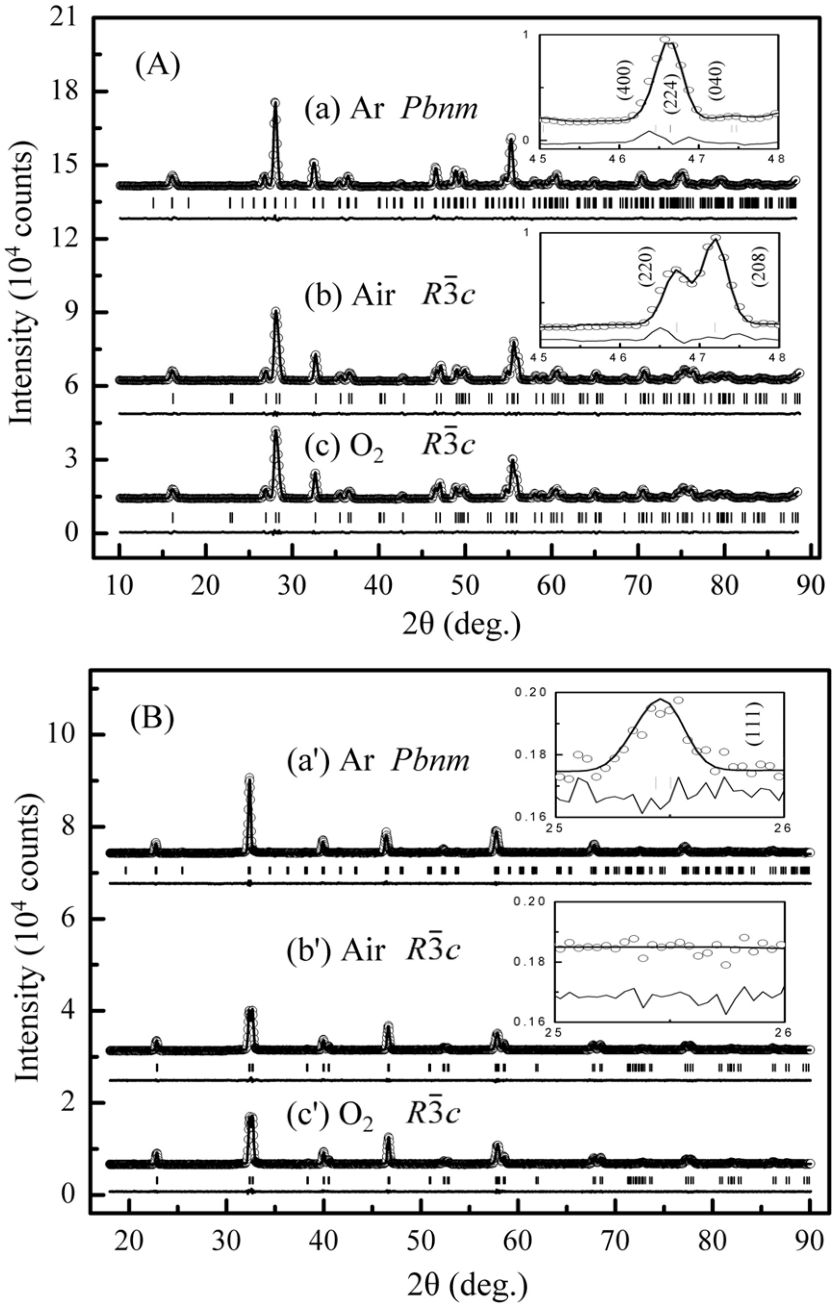

Figure 1. Observed (circles) and calculated (solid lines) patterns of neutron (A) and x-ray (B) powder diffraction diagrams for the Ar annealed (a) and (a′), air sintered (b) and (b′) and oxygen annealed (c) and (c′) $La_{0.875}Sr_{0.125}Mn_{1-\gamma}O_{3+\delta}$ samples at ambient conditions. The bars mark the positions of Bragg reflections. The lower curves in each panel represent the difference between the observed and calculated patterns. The insets show magnified patterns in certain 2θ regions.

between the equilibrium La(Sr)–O and Mn–O bond lengths, when the La(Sr) ions are too small to fill the space between MnO_6 octahedra, is given by the deviation of tolerance factor

Table 2. The summary of Curie temperature T_c, one-electron bandwidth W of the e_g band, relative concentration of cation vacancies in the B (Mn) sublattice V_B, tolerance factor t, number of nearest magnetic neighbours of Mn ions $z = 6(1-\gamma)$ and calculated Mn^{3+} and Mn^{4+} contents based on the charge neutrality condition for the Ar annealed, air sintered and oxygen annealed $La_{0.875}Sr_{0.125}Mn_{1-\gamma}O_{3+\delta}$ samples at room temperature. S is the sum of the spin quantum number of Mn^{3+} ($S = 2$) and Mn^{4+} ($S = 3/2$). Numbers in parentheses are the estimated standard deviation (e.s.d.) of the last significant digit.

Synthesis	Ar	Air	O_2
T_c (K)	192(1)	240(1)	237(1)
W ($10^{-4} \times$ Å$^{-3.5}$)	899.94(6)	930.66(1)	925.40(1)
V_B (%)	86	59	57
t	0.990(1)	0.993(1)	0.992(1)
$z = 6(1-\gamma)$	5.71(5)	5.74(5)	5.64(5)
Mn^{3+} (cn)	0.667(27)	0.639(26)	0.527(30)
Mn^{4+} (cn)	0.293(25)	0.347(24)	0.458(29)
Mn^{3+} (cn) (%)	69.5(26)	64.8(25)	53.5(30)
$S(S+1)$	4.9(3)	5.0(3)	4.8(3)
$2zS(S+1)$	56(3)	58(3)	54(4)

$t = \langle \text{La(Sr)–O} \rangle / \sqrt{2} \langle \text{Mn–O} \rangle$ from unity. When $t = 1$, the compound has an ideal perovskite structure. When $t < 1$, the Mn–O and La(Sr)–O bonds are subjected to compressive and tensile stresses, respectively. In order to relieve the internal chemical stress, the MnO_6 octahedra will cooperatively rotate and tilt to decrease the structure symmetry, thus leading to the R or O structure. Both increases of the ⟨Mn–O⟩ and ⟨La(Sr)–O⟩ bond lengths suggest that neither Mn–O nor La(Sr)–O directly controls the structural transition, but influences it indirectly through the tolerance factor. There are three kinds of Mn–O bond in the O structure: two Mn–O(2) in plane and one Mn–O(1) out of plane. Table 1 clearly shows the large differences between them, revealing a very strong Jahn–Teller distortion. The size of the Jahn–Teller distortion of MnO_6 octahedra can be evaluated by the following equation:

$$\Delta = \left(\frac{1}{6}\right) \sum_{n=1,6} \left[\frac{(d_n - \langle d \rangle)}{\langle d \rangle} \right]^2, \tag{3.1}$$

where $\langle d \rangle$ and d_n are the mean Mn–O bond length and the six Mn–O bond lengths along six different directions, respectively. The calculated Δ for the Ar annealed sample is $1.11(16) \times 10^{-4}$. With this distortion the t_{2g} state of the Mn^{3+} ions splits into three states (d_{xy}, d_{yz} and d_{zx}) and e_g state splits into two states ($d_{x^2-y^2}$ and $d_{3z^2-r^2}$). However, there is only one kind of Mn–O bond for the R structure, indicating almost no Jahn–Teller distortion and the retention of both t_{2g} and e_g states. The O–R transition related to an increase of the tolerance factor suppresses the Jahn–Teller distortion, which is accompanied by the increase of ⟨Mn–O–Mn⟩ bond angle from 161.08(4)° (Ar) to 163.38(1)° (O_2) and 163.64(1)° (air) (tables 1 and 2). The effective electron transfer interaction between neighbouring Mn ions is governed by the superexchange process via O 2p states. The relative value of the one-electron bandwidth W of the e_g band [13] can be estimated by

$$W \propto \frac{\cos \frac{1}{2}(\pi - \langle \text{Mn–O–Mn} \rangle)}{\langle \text{Mn–O} \rangle^{3.5}}. \tag{3.2}$$

The calculated values of W are listed in table 2. The flattening of MnO_6 octahedra caused by the O–R transition leads to an increase of the W value, in accordance with the estimated W values at the O–R phase boundary caused by hole doping [14]. There are two types of distortion

related to MnO_6 octahedra: one is the cooperative rotation corresponding to the ⟨Mn–O–Mn⟩ bond angle and tolerance factor, leading to structural transitions; another is the Jahn–Teller distortion that is inherent to the high-spin ($S = 2$) Mn^{3+} ions, which lifts the double degeneracy of e_g orbitals for the cubic environment, resulting in different Mn–O bond lengths. In the more strongly distorted O structure, the MnO_6 octahedra are tilted along the c direction, while in the weaker distortion (R structure), they are tilted almost along the [111] direction.

We have to point out that the synthesis conditions have a very important effect on the percentage of Mn^{3+} ions, i.e. $100 \times Mn^{3+}/(Mn^{3+} + Mn^{4+})$, through it seems that a high Mn^{4+} percentage, i.e. $100 \times Mn^{4+}/(Mn^{3+} + Mn^{4+})$, is stable at low preparation temperature regardless of the starting nominal compositions [15]. The Mn^{3+} and Mn^{4+} contents were evaluated from the refined site occupancies based on the charge neutrality condition (table 2). As the oxygen content decreases, the percentage of Mn^{3+} ions increases. This correlation suggests that the Jahn–Teller distortion caused by the R–O transition promotes Mn^{3+} ions: as the Mn^{4+} percentage decreases with the decrease of oxygen content, the Mn^{3+} percentage increases, as does the Jahn–Teller distortion. The high percentage of Mn^{4+} ions compensates for the lack of positive charge in the deficient cation sites and the abundance of negative charge in the oxygen sites.

4. Magnetic properties

In order to explore the effect of Ar and O_2 annealings on the magnetic properties, we performed magnetization measurements from 5 to 400 K in dc fields of 20 and 60 Oe. The ZFC and FC magnetizations as a function of temperature at an applied field of 20 Oe for three samples are shown in figure 2(a). With decreasing temperature, the transitions from paramagnetism to ferromagnetism at T_c are continuous and sharp, indicating a good sample quality with homogeneous composition. The signatures of structural transitions reported for $La_{0.875}Sr_{0.125}MnO_3$ single crystal [7] are not present in our magnetization data. These features were only observed for single-crystal but not for polycrystalline samples. The FC magnetization for the Ar and O_2 annealed samples is larger and smaller than that of the air sintered sample, respectively, which indicates that the Ar and O_2 annealings have changed the magnetic states, e.g. the ratio of Mn^{3+}/Mn^{4+} or the domain structures, etc. Compared with the air sintered sample, the widths of the ferromagnetic transition for Ar and O_2 annealed samples are slightly larger, especially for the Ar annealed sample, indicating a slightly broader distribution of the exchange coupling strength between Mn ions. From the inflection point of ZFC curves, we determined the Curie temperature T_c as listed in table 2. Thermomagnetic irreversibilities are observed as differences between the ZFC and FC curves for three samples. This is especially pronounced for the O_2 and Ar annealed samples, indicating a less homogenous ferromagnetic order. At ∼230 K, just below $T_c = 237$ K, the ZFC magnetization of O_2 annealed sample has a well-defined peak and it continuously decreases towards the lower temperatures, while the FC magnetization is nearly constant below 230 K. Although spin glasses show similar irreversibilities, our study of the magnetization relaxation at 20 K shows no time dependence, and we thus conclude that the behaviour comes from the ferromagnetic domain structures. Similar phenomena are observed for the Ar annealed sample, where we also could not detect any time dependence at $T = 60$ K, and the FC magnetization continuously rises from 192 (T_c) to 5 K. For a deeper understanding of the irreversibilities, ac susceptibility studies as functions of frequency and field have to be conducted. However, that goes beyond the scope of the present paper. Figure 2(b) shows ZFC $M(T)$ curves of the Ar annealed sample at applied fields of 20 and 60 Oe. An interesting feature is that the ZFC magnetization at 60 Oe has two peaks at 145 and 175 K, respectively. In the temperature

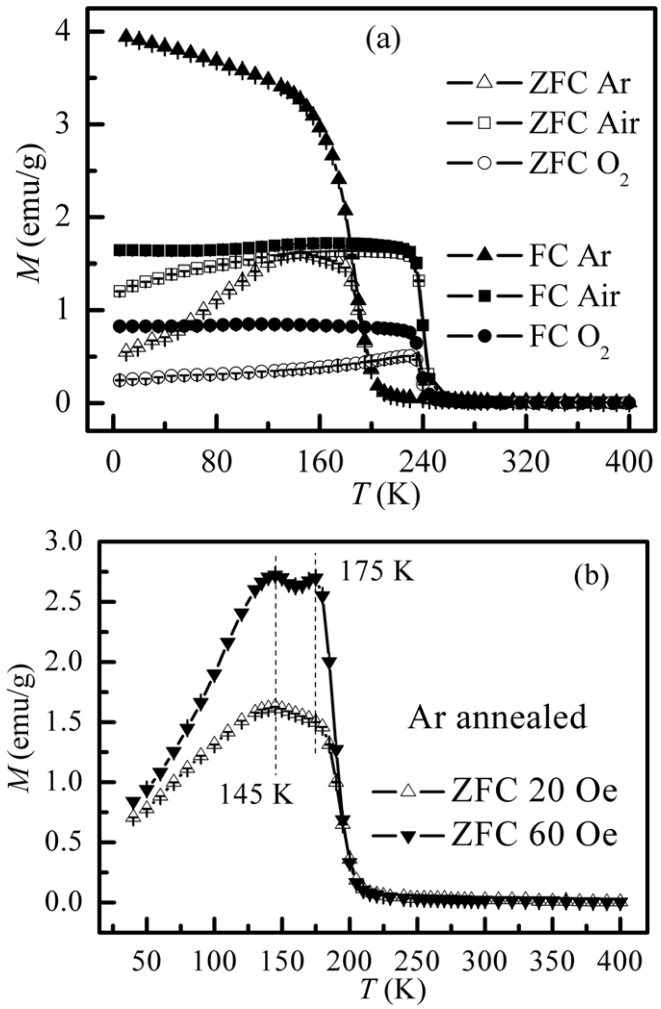

Figure 2. ZFC and FC magnetization M versus temperature measured at $H = 20$ Oe for three $La_{0.875}Sr_{0.125}Mn_{1-\gamma}O_{3+\delta}$ samples (a), and ZFC M at 20 and 60 Oe for the Ar annealed sample (b). The lines are guides to the eye.

ranges 145 K $< T <$ 159 K and 159 K $< T <$ 175 K, the value of magnetization decreases and increases, respectively, which corresponds to the behaviour observed in the single crystal [7], where well-defined transitions at T_{JT}, T_c and $T_{O'O''}$ are observed. According to [7], at $T_c \approx 180$ K a canted magnetic structure appears and at the temperature of the O′–O″ transition ($\sim$140 K) the magnetization increases again. Our polycrystalline sample thus shows some typical features characteristic for single crystals with the same nominal composition.

5. Discussion

The refined site occupancies show all samples contain excess oxygen. Many papers [16–19] have reported the so-called 'excess oxygen' problem for manganites, especially when the reaction temperature is relative low, but few of them gave the reasons. Oxygen

nonstoichiometry has been found in $La_{1-x}Sr_xMnO_{3+\delta}$ perovskites ($x = 0.0$–0.5) prepared in the temperature range from 873 to 1273 K [12]. For our samples, when the reaction temperature is below 1373 K, XPD spectra always evidence traces of $La(OH)_3$ formed from the residual La_2O_3 in reactants through absorbing moisture in air below 423 K (TGA). Our XPD experiment shows that the transition from La_2O_3 to $La(OH)_3$ has completed after the exposure of pure La_2O_3 to air for ∼2 h, which of course depends on the moisture capacity in the air. If the composition of this kind of sample is measured by chemical analysis, it shows obviously excess oxygen, part of which definitely comes from the above transition. It is uncertain that this kind of sample contains unreacted Sr or Mn compounds if their amounts are beyond the detection limit of the method. Such an uncompleted reaction results in non-stoichiometric manganites, e.g. the La site deficiency and the increase of Mn^{4+} percentage, T_c and oxygen content. In our case, we are confident that the reaction has completed above 1473 K because we have never detected traces of unreacted La, Sr or Mn compounds. Even after one month's exposure to air, the XPD pattern and the ZFC magnetization have not changed. Since the speed of chemical reaction depends on the temperature and the particle size of reactants, it is suggested that the reaction temperature should be high enough. However, at the same time the problem of sublimation becomes more severe, especially for the calcination step. Most of the manganites are synthesized through solid state reactions at high temperatures. Thus it seems that the appearance of excess oxygen in $La_{1-x}Sr_xMnO_3$ at low doping levels is unavoidable for the conventional preparation method.

In refinements, the oxygen site occupancy turns out to be larger than the nominal value of 3 for all samples. The excess oxygen is not accommodated in interstitial sites, i.e. (1/2, 0, 0) of the primitive perovskite cube and (1/4, 1/4, 1/4) in the LaO_3 sublattice. Thus this is an artefact since the perovskite sites ($Pbnm$: 4c and 8d; $R\bar{3}c$: 6e) cannot accommodate additional oxygen. This artefact arises from the fact that the La and Sr site occupancies were arbitrarily fixed to be the stoichiometric values of 0.875 and 0.125, respectively. Therefore the observed oxygen deviation from the nominal stoichiometry should be interpreted as cation vacancies in the A (La and Sr) and B (Mn) sublattices, which will be present at elevated preparation temperatures. Using neutron diffraction and high-resolution transmission electron microscopy methods, Van Roosmalen *et al* [17] suggested that the actual composition was $La_{0.95}Mn_{0.95}O_3$ with equal amount of vacancies in the La and Mn sublattices for the formal $LaMnO_{3.158}$ sample. From simultaneous x-ray and neutron Rietveld refinement, we have arrived at a similar conclusion: the formula of $La_{0.875-\alpha}Sr_{0.125-\beta}Mn_{1-\gamma}O_{3+\delta}$ should be written as $La_{0.875-\alpha'}Sr_{0.125-\beta'}Mn_{1-\gamma'}O_3$, but the hole concentration does not change because of the charge neutrality condition. Based on the joint refinements with different models and the above discussion the actual formulae of Ar annealed, air sintered and O_2 annealed samples are $La_{0.868(1)}Sr_{0.124(1)}Mn_{0.952(8)}O_3$(Ar), $La_{0.850(1)}Sr_{0.121(1)}Mn_{0.957(8)}O_3$(air) and $La_{0.835(2)}Sr_{0.119(1)}Mn_{0.940(8)}O_3(O_2)$, respectively. To compare the actual distributions of cation vacancies in the A (La and Sr) and B (Mn) sublattices, we express the formulae as $A_{0.992(2)}B_{0.952(8)}O_3$ (Ar), $A_{0.971(1)}B_{0.957(8)}O_3$ (air) and $A_{0.954(2)}B_{0.940(8)}O_3$ (O_2). For all three samples, we thus observe more vacancies in the B (V_B''') sublattice than that in the A (V_A''') sublattice. We define the relative concentration of cation vacancies in the B sublattice compared to the sum of cation vacancies in the A and B sublattices as $V_B(\%) = 100 \times V_B'''/(V_A''' + V_B''')$ and the calculated values of V_B for all samples are shown in table 2. It is possible that as V_B increases, T_c decreases and the ferromagnetic transition becomes slightly wider (figure 2(a)). An increase of the B sublattice vacancies leads to a decrease of the strength of magnetic exchange interaction and a widening of its distribution. The effects of the presence and distribution of cation vacancies in $(La, M)MnO_{3+\delta}$ (where M = Na, Ca) on their magnetic properties were recently reported [18]; however, the usual parameters, e.g. Mn–O–Mn bond

angle and Mn–O bond length, fail to explain the trend of T_c there. Obviously, only the purely geometrical factor is not sufficient to explain the surprising change of T_c.

To investigate the reasons for the decrease of the Mn site occupancy in Ar and O_2 annealed samples in more detail, studies were conducted with a TGA instrument and an actual furnace with subsequent ICP-OES analysis. We could show that the flowing gas significantly accelerates the reaction compared with the static conditions. In addition, it favours the sublimation of elements. It should be stressed that the Ar and O_2 annealed samples experienced one more firing, mixing and milling than the air sintered sample. To conclude, the Ar and O_2 annealings in the present case can lead to a decrease and an increase of the oxygen site occupancy, respectively, and at the same time may accompany the decrease of Mn ions. Similar behaviour was also suggested in [19].

We attempted to explore the effects of Ar and O_2 annealings on T_c of $La_{0.875}Sr_{0.125}Mn_{1-\gamma}O_{3+\delta}$ and establish the possible correlations between their structural and magnetic properties among the various parameters. The Curie temperature of a Heisenberg ferromagnet with nearest-neighbour interactions only is given in the molecular field approximation as

$$T_c = 2zJS(S+1)/3k_B. \tag{5.1}$$

Equation (5.1) shows that there are three influencing factors determining the value of T_c and all of them are listed in table 2: (i) the number of nearest magnetic neighbours z ($z = 6(1-\gamma)$); (ii) the spin quantum number S, depending on the Mn content and Mn valence state (Mn^{3+}: $S = 2$; Mn^{4+}: $S = 3/2$); and (iii) the exchange constant J. As can be seen from table 2, the value of $2zS(S+1)$ is almost the same for three samples within the e.s.d. The exchange constant J depends on the ⟨Mn–O–Mn⟩ bond angle and ⟨Mn–O⟩ bond length. As can be seen from equation (3.2), the one-electron bandwidth W of the e_g band can be used as a measure for the strength of ferromagnetic double-exchange interaction between Mn^{3+} and Mn^{4+} ions. Indeed, we find a nearly linear dependence between W and T_c for three samples, which indicates that the exchange constant J is the most important determining factor for the drastic differences in T_c for all samples (table 2).

In order to investigate the individual effect of the number of nearest magnetic neighbours z on the structural and magnetic properties in detail, another control experiment was performed using a set of $La_{0.875}Sr_{0.125}Mn_yO_3$ samples with initial $y = 0.97$, 1.00 and 1.03. Following the general procedure for sample preparation given above, these $La_{0.875}Sr_{0.125}Mn_yO_3$ samples were simultaneously calcined three times at 1073, 1273 and 1473 K, respectively, for 12 h, and sintered only once at 1573 K for 12 h in air. Every sample is a single phase within the detecting limitation of XPD method. Although XPD is not very sensitive to the oxygen structural parameters, the Mn site occupancy can still be determined reliably, as we verified by different refining procedures. The refined structural parameters are listed in table 3. Though the crystal structure for all three $La_{0.875}Sr_{0.125}Mn_yO_3$ samples is R, the structural distortion decreases as the decrease of α_{rhomb} from 60.619(1)° to 60.612(1)°, and to 60.603(1)° for initial $y = 0.97$, 1.00 and 1.03, respectively. The refined Mn site occupancy is reduced by ∼1.8% and ∼4.1% for the samples with initial $y = 1.00$ and 0.97, respectively, compared to that of $La_{0.875}Sr_{0.125}Mn_yO_3$ with initial $y = 1.03$. This is consistent with the initial compositions and high-temperature reactions. The calculated numbers of nearest magnetic neighbours z obtained from the refined Mn site occupancies are shown in table 3. The decrease of the relative Mn site occupancy results in the decrease of unit-cell volume V per Mn ion and lowers the value of z. Figure 3 shows the ZFC magnetization measured at an applied field of 20 Oe for three $La_{0.875}Sr_{0.125}Mn_yO_3$ samples. Again, it can be seen that the cationic nonstoichiometry, especially for the B (Mn) sites, has a very significant effect on the magnetic properties. The Curie temperature T_c is reduced by ∼11.9% and ∼23.4% for the samples with

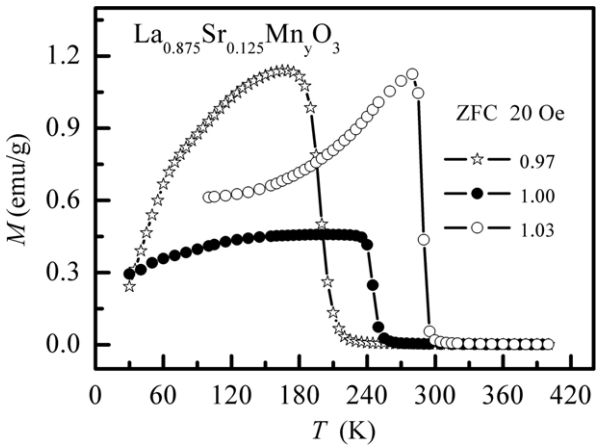

Figure 3. ZFC magnetization M versus temperature measured at $H = 20$ Oe for the three air sintered $La_{0.875}Sr_{0.125}Mn_yO_3$ samples with initial $y = 0.97$, 1.00 and 1.03, belonging to the rhombohedral structure at room temperature. The solid lines are guides to the eye.

Table 3. Refined structural parameters of the three air sintered $La_{0.875}Sr_{0.125}Mn_yO_3$ samples with initial $y = 0.97$, 1.00 and 1.03 as obtained from refinements of XPD data, and the summary of Curie temperature T_c and number of nearest magnetic neighbours of Mn ions $z = 6(1 - \gamma)$. μ represents the refined Mn site occupancy. Numbers in parentheses are the estimated standard deviation (e.s.d.) of the last significant digit.

Synthesis	0.97	1.00	1.03
Crystal system	R	R	R
Space group	$R\bar{3}c$	$R\bar{3}c$	$R\bar{3}c$
T_c (K)	226(1)	260(1)	295(1)
$\mu_{refining}$ (Mn)	0.970(4)	0.993(3)	1.012(4)
$z = 6(1 - \gamma)$	5.82(3)	5.96(2)	6.07(3)
$a = b = c$ (Å)	5.4755(1)	5.4799(1)	5.4857(1)
α_{rhomb} (deg)	60.619(1)	60.612(1)	60.603(1)
V_{cell}/Mn (Å^3)	58.85(1)	58.98(1)	59.16(1)
R_p (%)	2.65	3.46	3.96
R_{wp} (%)	3.46	4.48	5.08
χ^2	1.37	1.19	1.09

initial $y = 1.00$ and 0.97, respectively, compared to that of $La_{0.875}Sr_{0.125}Mn_yO_3$ with initial $y = 1.03$. Obviously, the strong decrease of T_c from 295(1) K to 260(1) K, and to 226(1) K for initial $y = 1.03$, 1.00 and 0.97, respectively, is largely due to a decrease in Mn content and thus a decrease of the number of nearest magnetic neighbours z.

To summarize, the structural and magnetic properties are strongly dependent on the sample synthesis conditions. The decrease of the total strength of magnetic interactions resulting from a decrease of the single-electron bandwidth W, or the decrease of Mn content, can lead to a drastic decrease of the Curie temperature.

6. Conclusions

In the present paper, we have systematically studied the effects of Ar and O_2 annealings on $La_{0.875}Sr_{0.125}Mn_{1-\gamma}O_{3+\delta}$ manganites with a fixed Sr doping. The structural parameters

(lattice constants, atomic coordinates and site occupancies) of air sintered, Ar and O_2 annealed samples were refined. The $La_{0.875}Sr_{0.125}Mn_{1-\gamma}O_{3+\delta}$ samples have been found to exhibit either an orthorhombic (Ar annealed) or a rhombohedral structure (air sintered and O_2 annealed). Depending on the firing atmospheres (air, Ar or O_2), cation vacancies are present in the samples, which lead to drastic changes of the magnetic properties. The one-electron bandwidth W of the e_g band, the actual concentration of vacancies in the B (Mn) sublattice V_B and the number of nearest magnetic neighbours are correlated with the decrease of T_c. In conclusion, our results clearly demonstrate how an extremely small change in the stoichiometry can have huge effects on the structural and magnetic properties in these compounds based on the perovskite structure. Comparing the Ar annealed with the air sintered $La_{0.875}Sr_{0.125}Mn_{1-\gamma}O_{3+\delta}$ sample, only a $\sim$2.2% relative decrease of oxygen content can lead to a structural transition from rhombohedral to orthorhombic and to a decrease of the magnetic transition temperature by $\sim$20%. Such a huge response on small changes of parameters is characteristic of this complex system. Only a combined refinement of x-ray and neutron diffraction data allows one to determine the stoichiometry with the required precision to be able to compare results from different samples.

Acknowledgments

The authors are grateful to Mr H Braak for his kind help with the SQUID measurements. We also acknowledge ZCH (Central Division of Analytical Chemistry) of Research Center Jülich GmbH, Germany, for the measurement of cationic contents.

References

[1] Hemberger J, Krimmel A, Kurz T, Krug von Nidda H A, Ivanov V Y, Mukhin A A, Balbashov A M and Loidl A 2002 *Phys. Rev.* B **66** 094410
[2] Su Y, Istomin K, Wermeille D, Fattah A, Foucart P, Meuffels P, Hupfeld D and Brueckel Th 2004 *J. Magn. Magn. Mater.* **272** 291
[3] Liu G L, Zhou J S and Goodenough J B 2001 *Phys. Rev.* B **64** 144414
[4] Jung J H, Kim K H, Lee H J, Ahn J S, Hur N J and Noh T W 1999 *Phys. Rev.* B **59** 3793
[5] Argyriou D N, Mitchell J F, Potter C D, Hinks D G, Jorgensen J D and Bader S D 1996 *Phys. Rev. Lett.* **76** 3826
[6] Dutta A, Gayathri N and Ranganathan R 2003 *Phys. Rev.* B **68** 054432
[7] Paraskevopoulos M, Mayr F, Hartinger C, Pimenov A, Hemberger J, Lunkenheimer P, Loidl A, Mukhin A A, Ivanov V Y and Balbashov A M 2000 *J. Magn. Magn. Mater.* **211** 118
[8] Geck J, Wochner P, Kiele S, Klingeler R, Revcolevschi A, Zimmermann M V, Buechner B and Reutler P 2004 *New J. Phys.* **6** 152
[9] Endoh Y, Hirota K, Ishihara S, Okamoto S, Murakami Y, Nishizawa A, Fukuda T, Kimura H, Nojiri H, Kaneko K and Maekawa S 1999 *Phys. Rev. Lett.* **82** 4328
[10] Yamada Y, Suzuki J, Oikawa K, Katano S and Fernandez-Baca J A 2000 *Phys. Rev.* B **62** 11600
[11] Schaefer W, Jansen E, Skowronek R and Kirfel A 1997 *Physica* B **234–236** 1146
[12] Rodriguez-Carvajal J 1993 *Physica* B **192** 55
[13] Medarde M, Mesot J, Lacorre P, Rosenkranz S, Fischer P and Gobrecht K 1995 *Phys. Rev.* B **52** 9248
[14] Xu S, Moritomo Y, Ohoyama K and Nakamura A 2003 *J. Phys. Soc. Japan* **72** 709
[15] Mitchell J F, Argyriou D N, Potter C D, Hinks D G, Jorgensen J D and Bader S D 1996 *Phys. Rev.* B **54** 6172
[16] Mizusaki J, Tagawa H, Naraya K and Sasamoto T 1991 *Solid State Ion.* **49** 111
[17] Van Roosmalen J A M, Cordfunke E H P and Helmholdt R B 1994 *J. Solid State Chem.* **110** 100
[18] Malavasi L, Ritter C, Mozzati M C, Tealdi C, Islam M S, Azzoni C B and Flor G 2005 *J. Solid State Chem.* **178** 2042
[19] Itoh M, Nishi K, Yu J D and Inaguma Y 1997 *Phys. Rev.* B **55** 14408